CHAPTER 6

REDUCED GRAPHENE OXIDE-POLYANILINE NANOTUBES NANOCOMPOSITE ELECTRODE SYSTEM

This chapter focuses on the synthesis of reduced graphene oxide-polyaniline nanotubes nanocomposites with varying concentration of reduced graphene oxide by an in-situ reduction method. The physico-chemical properties of the synthesized nanocomposites and their constituent components have been investigated by various characterization techniques such as HRTEM, XRD, FTIR and micro-Raman spectroscopy. The electrochemical charge storage parameters of the nanocomposites such as specific capacitance, coulombic efficiency, energy density, power density and cycle life have been investigated by cyclic voltammetry and galvanostatic charge-discharge measurements. The electrode-electrolyte interfacial resistance for the pristine and nanocomposite electrodes has been evaluated using electrochemical impedance spectroscopy.

6.1 Introduction

One-dimensional nanostructures (e.g. nanorods, nanofibers, nanotubes etc.) of conducting polymers (CPs) have been widely studied in supercapacitor applications due to their high specific capacitance, high energy density, and easy processability [327]. These nanostructures have the ability to store charges by faradaic charge transfer reactions on the electrode surface known as pseudocapacitance and also provide shorter pathways for ion diffusion [42, 161], which improves the electrochemical performance. However, the repeated faradaic reactions on the electrode surface reduce their cyclic stability and limit their application. To overcome these shortcomings, CPs have been coupled with different carbonaceous materials like graphene and its derivatives, activated carbons, carbon nanotubes and fullerenes to obtain electrode materials with high specific capacitance and good cyclic stability [328, 329]. These carbon materials can store charges electrostatically

in electrical double layers across the electrode-electrolyte interface, which is known as electric double layer capacitance (EDLC) [330]. Among these materials, graphene is the most preferred secondary counterpart within CP nanostructures but it is difficult to process graphene sheets in large quantities due to their easy agglomeration and restacking. Therefore, reduced graphene oxide (RGO), a derivative with a few layers of graphene has been considered for dispersion within various CPs where the CP nanostructures can provide pseudocapacitance as well as act as spacers to prevent the restacking of RGO nanosheets [122]. RGO possesses a net negative charge due to the residual oxygen containing groups in its basal plane and edge. Negatively charged RGO can bind with CPs through electrostatic attractions as CPs become positively charged upon oxidation giving rise to enhanced performance of the nanocomposite electrode [331].

In this chapter, nanocomposites of RGO and polyaniline nanotubes (PAniNTs) have been synthesized by *in situ* reduction of GO in presence of PAniNTs to suppress the agglomeration of RGO. Four nanocomposites have been prepared by varying the concentration of GO with respect to PAniNTs. The detailed synthesis procedure and sample compositions have been discussed in section 3.3 of Chapter 3. The morphology, structure and thermal stability of the pristine components and the nanocomposites have been studied by HRTEM, XRD, FTIR, micro-Raman and thermogravimetric measurements. Electrical properties of the nanocomposites have been investigated by two-probe current-voltage and four-probe conductivity measurements. The electrochemical charge storage properties of the nanocomposites have been studied by cyclic voltammetry, galvanostatic charge-discharge measurements and electrochemical impedance spectroscopy. The cyclic stability of the nanocomposites upto 1000 cycles has been evaluated and compared with that of PAniNTs.

6.2 Structural characterization

6.2.1 Morphological analysis

The HRTEM micrographs of RGO, PAniNTs and RGO-PAniNTs nanocomposites are shown in Figure 6.1. The HRTEM image of RGO displays a sheet-like morphology with wrinkles on the surface indicating that the sheets are thin. Figure 6.1 (b) shows the morphology of polyaniline where a hollow tubular structure is

observed whose average outer diameter is measured to be around 134 nm. The HRTEM micrographs of the nanocomposites display a nanosized structure of both the components RGO and PAniNTs, which signifies the successful formation of the nanocomposites. Homogeneous dispersion of RGO and PAniNTs is observed in the nanocomposites in the low as well as high RGO loading and the RGO nanosheet retains its original layer-like structure. RGO due to the presence of residual oxygen containing groups carries a net negative charge in its structure and PAniNTs carry a positive charge upon oxidation. PAniNTs and RGO sheets assemble due to the electrostatic attraction between the two components. This demonstrates that PAniNTs present on the surface of RGO nanosheets as observed from the micrographs are capable of preventing the aggregation of RGO nanosheets and act as spacers during the reduction process. This is possibly due to *in situ* reduction of GO in presence of PAniNTs.

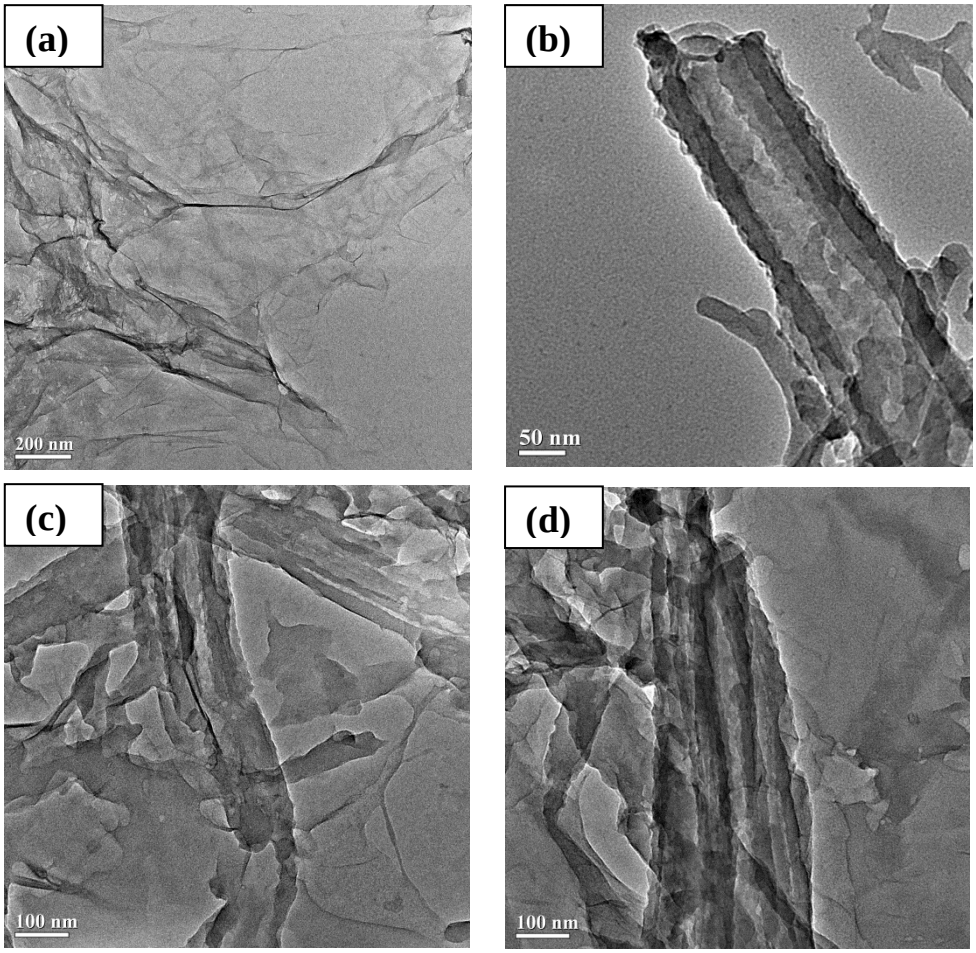

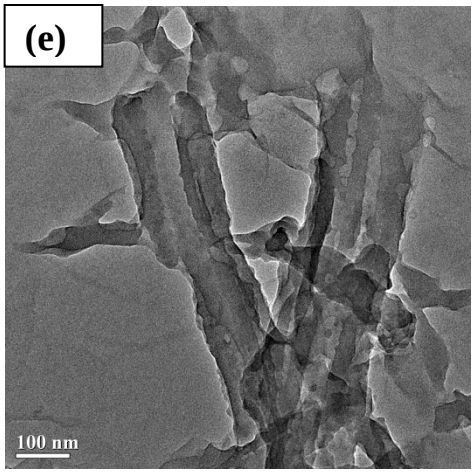

Figure 6.1: *HRTEM micrographs of (a) RGO nanosheets, (b) PAniNTs and RGO-PAniNTs nanocomposites with (c) 5 wt. %, (d) 20 wt. % and (e) 40 wt. % of RGO.*

6.2.2 X-ray diffraction analysis

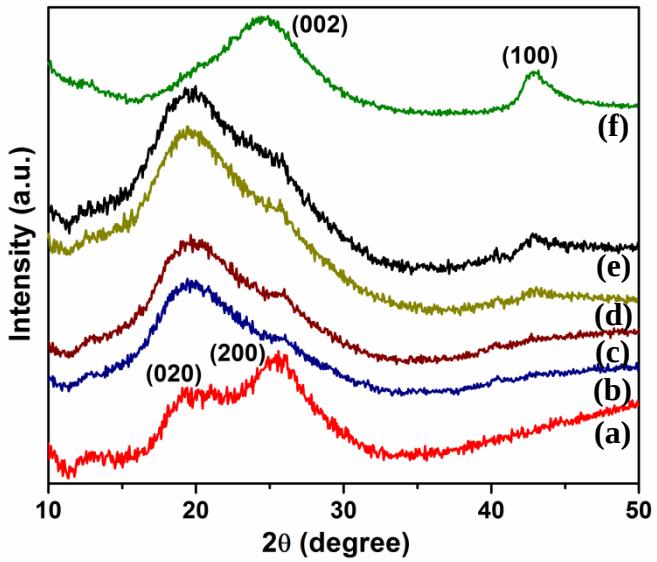

Figure 6.2: *X-ray diffractograms of (a) PAniNTs and RGO-PAniNTs nanocomposites with (b) 5 wt. %, (c) 10 wt. %, (d) 20 wt. %, (e) 40 wt. % of RGO and (f) RGO.*

The X-ray diffractograms of RGO, PAniNTs and RGO-PAniNTs nanocomposites are shown in Figure 6.2. The XRD pattern of RGO exhibits two broad peaks at 2θ = 24.6° and 43°. The first peak corresponds to a d-spacing of 0.36 nm along the (002) orientation and the second peak is due to the reflection of (100) crystallographic plane, respectively [332]. The broad nature of the RGO peaks indicates the partial

exfoliation of the RGO layers. PAniNTs exhibit two broad diffraction humps centered at 2θ = 19.4° and 25° corresponding to (020) and (200) crystal planes of PAni, which suggests that the resulting PAniNTs are semi-crystalline in nature. The semi-crystalline nature of PAniNTs originates from the local ordering of PAni chains, which are separated by structural disorder. These two peaks are due to the scattering from the periodicity parallel and perpendicular to the polymer chains of PAni, respectively [333]. The RGO-PAniNTs nanocomposites show a broad peak at 2θ range of 15°-28°, which is attributed to overlapping of the (002) peak of RGO with the (020) and (200) peaks of PAniNTs. The shoulder peak appearing at 2θ = 25° is due to the (200) diffraction plane of PAniNTs. As the concentration of RGO is increased to 20 wt. %, an additional diffraction peak at 2θ = 43° corresponding to (100) plane of RGO is observed, which becomes more prominent for 40 wt. % of RGO loading. This indicates the successful reduction of GO in the nanocomposites in presence of PAniNTs. However, the peak is not observed below 20 wt. % of RGO which may be due to the low content of RGO in the nanocomposites. The relative crystallinity percentage (X_c) of PAniNTs and the nanocomposites has been calculated using the following equation:

$$X_c = \left[\frac{A_c}{A_c + A_a}\right] \times 100\ \% \qquad (6.1)$$

where, A_c is the area of the crystalline domain and A_a is the area of the amorphous region. The relative crystallinity of PAniNTs and the nanocomposites with 5, 10, 20 and 40 wt. % of RGO is calculated to be 26.8, 31.7, 34.7, 42.2 and 44.6%, respectively. The increased % crystallinity of the nanocomposites with increase in RGO concentration is attributed to the increasing amount of crystalline phase i.e. RGO within the nanocomposites.

6.3 Vibrational spectroscopy

6.3.1 Fourier transform infrared spectroscopy

The FTIR spectra of RGO, PAniNTs and RGO-PAniNTs nanocomposites in the range of 400-4000 cm^{-1} are shown in Figure 6.3. The FTIR spectrum of RGO exhibits absorbance at 1628 cm^{-1} due to C=C sp^2 bonds [283]. The peak appearing at 1023 cm^{-1} is attributed to C-O stretching vibrations, which reveals the presence of partial oxygen groups in RGO [334]. In the FTIR spectra of PAniNTs, the

characteristic absorption bands appear at 1562 and 1477 cm^{-1} corresponding to the stretching vibration of C=C in quinoid and benzenoid rings, respectively. These two characteristic bands indicate the emaraldine salt form of PAni [335]. Strong bands at 1292 and 1107 cm^{-1} are designated as the C-N stretching mode of secondary aromatic amine and aromatic C-H in-plane bending [336, 337]. The peak at 795 cm^{-1} is assigned to the C-H out-of-plane deformation of PAni [338]. The FTIR spectra of RGO-PAniNTs nanocomposites have similar characteristic bands as that of PAniNTs. However, shifting of bands at 1562, 1477, 1107 and 795 cm^{-1} of PAni has been observed towards higher wave numbers to 1587, 1496, 1130 and 814 cm^{-1}, respectively in the nanocomposites. The shifting can be ascribed to the change in chemical environment in the nanocomposites due to π-π interaction between PAni chains and RGO nanosheets. A broad absorption peak at 3438 cm^{-1} corresponding to O-H stretching vibrations is observed both for RGO and PAniNTs due to residual water molecules, which overlaps in the FTIR spectra of the nanocomposites [339]. The bands associated with aliphatic CH and CH_2 groups are observed at 2853 and 2924 cm^{-1}, respectively in the spectrum of RGO, PAniNTs as well as in the nanocomposites [340]. Table 6.1 presents the IR bands of PAniNTs and RGO along with their respective positions.

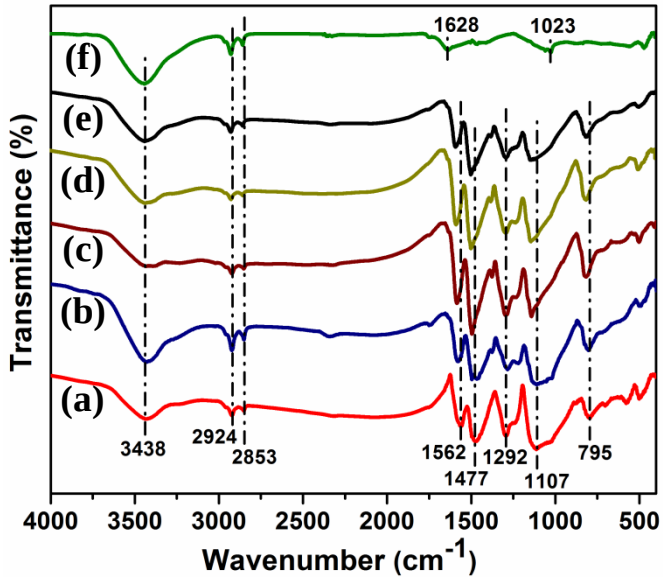

Figure 6.3: *FTIR spectra of (a) PAniNTs and RGO-PAniNTs nanocomposites with (b) 5 wt. %, (c) 10 wt. %, (d) 20 wt. %, (e) 40 wt. % of RGO and (f) RGO.*

Table 6.1: *Characteristic IR bands of PAniNTs, RGO and their assignments*

IR Bands	**Assignments**
PAniNTs	
795 cm^{-1}	C-H out-of-plane deformation [338]
1107 cm^{-1}	C-H in-plane bending [337]
1292 cm^{-1}	C-N stretching [336]
1477, 1562 cm^{-1}	C=C stretching in benzenoid and quinoid rings [335]
2853, 2924 cm^{-1}	CH and CH_2 stretching [340]
3438 cm^{-1}	O-H stretching [339]
RGO	
1023 cm^{-1}	C-O stretching [334]
1628 cm^{-1}	C=C stretching [283]
2853, 2924 cm^{-1}	CH and CH_2 stretching [340]
3438 cm^{-1}	O-H stretching [339]

6.3.2 Micro-Raman spectroscopy

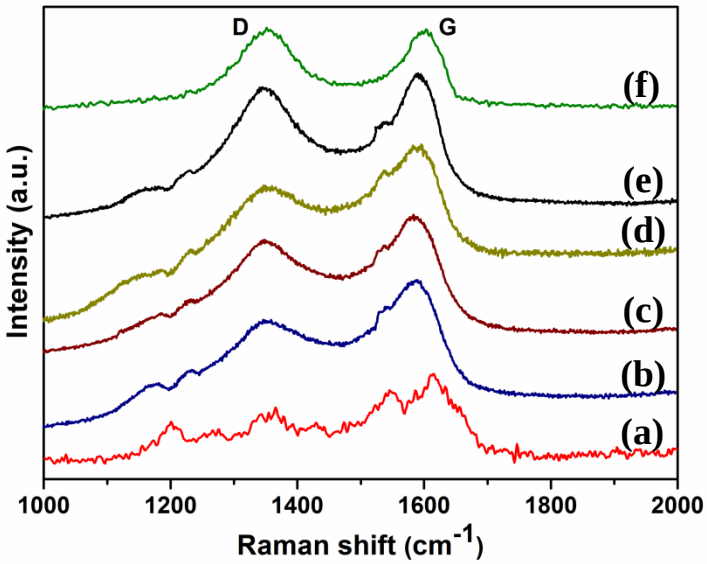

Figure 6.4: *Micro-Raman spectra of (a) PAniNTs and RGO-PAniNTs nanocomposites with (b) 5 wt. %, (c) 10 wt. %, (d) 20 wt. %, (e) 40 wt. % of RGO and (f) RGO.*

The micro-Raman spectra of RGO, PAniNTs and RGO-PAniNTs nanocomposites in the range of 1000-2000 cm^{-1} are presented in Figure 6.4. The micro-Raman spectrum

of RGO displays two prominent bands at 1355 and 1595 cm^{-1}, which corresponds to D and G bands. The G band is related to the stretching vibration of sp^2-hybridized carbon atoms, while the D band corresponds to the breathing of carbon rings that become Raman active due to a loss in translational symmetry. The presence of D band indicates defects and partially disordered structure of RGO created by the hydroxyl and epoxide groups on the carbon basal plane which is a well noticed phenomenon in chemically synthesized RGO [341]. The Raman spectra of PAniNTs display all its characteristic peaks, which suggests the successful formation of PAniNTs from templates of MnO_2 nanotubes. The band at 1196 cm^{-1} is assigned to the C-H bending of the quinoid or benzenoid ring [342]. The bands located at 1266 and 1350 cm^{-1} are attributed to C-N stretching of benzene-diamine units and $C\text{-}N^{+\cdot}$ stretching of the bipolaron structure [343]. C=C stretching mode of the quinoid ring and C-C stretching of the benzenoid ring are observed at 1544 and 1608 cm^{-1}, respectively [344]. Compared to the spectrum of pure PAniNTs, the C-H bending and the C-N stretching peak is red shifted to 1180 and 1233 cm^{-1} in the nanocomposites, which indicates a change in chemical environment of the C-H and C-N bands in the nanocomposite during the *in situ* formation of RGO. This shifting could be attributed to electron cloud delocalization of C-H and C-N bands in the nanocomposite structure due to the presence of RGO. The C-C stretching of the quinoid ring is observed as a small shoulder in the nanocomposites. The D and G bands of RGO are found to overlap with the PAni peaks located at 1350 cm^{-1} and 1608 cm^{-1}, respectively. It is noticed that the intensity of the PAni peaks decreases in the nanocomposites, which may be due to the interactions between the two components. The characteristic micro-Raman peaks of PAniNTs and RGO with their corresponding peak positions have been assigned in Table 6.2.

Table 6.2: *Characteristic micro-Raman bands of PAniNTs, RGO and their assignments*

Raman Bands	**Assignments**
PAniNTs	
1196 cm^{-1}	C-H bending of quinoid or benzenoid ring [342]
1266 cm^{-1}	C-N stretching of benzene-diamine units [342, 343]
1350 cm^{-1}	$C\text{-}N^{+\cdot}$ stretching of bipolaron structure [342, 343]

1544 cm^{-1}	C=C stretching of quinoid ring [342, 344]
1608 cm^{-1}	C-C stretching of benzenoid ring [342, 344]
RGO	
1355 cm^{-1}	D band: breathing mode from sp^2 carbon rings [288]
1595 cm^{-1}	G band: in-plane sp^2 C-C stretching [289]

6.4 Thermogravimetric analysis

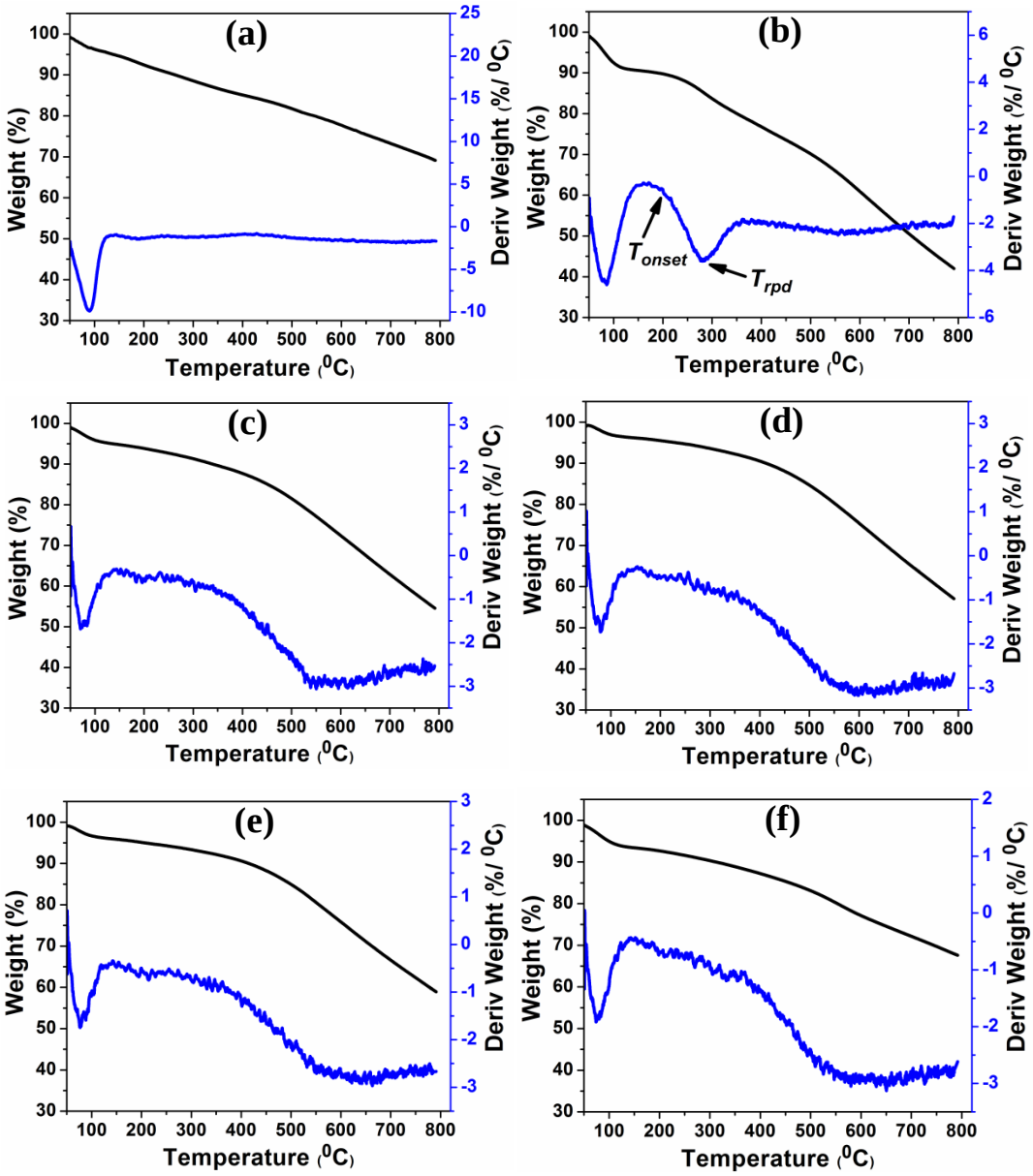

Figure 6.5: *TG and derivative of TG curves of (a) RGO, (b) PAniNTs and RGO-PAniNTs nanocomposites with (c) 5 wt. %, (d) 10 wt. %, (e) 20 wt. % and (f) 40 wt. % of RGO.*

The thermogravimetric (TG) curves of RGO, PAniNTs and RGO-PAniNTs nanocomposites within the temperature range of 50-800 °C are shown in Figure 6.5. All the samples show a weight loss below 100 °C due to the loss of residual moisture in the sample. The thermogram of PAniNTs exhibits a major weight loss around 200 °C, which is attributed to the degradation of the PAni backbone [345]. Pristine RGO exhibits a slow degradation, corresponding to the decomposition of remaining oxygen functional groups, such as –OH, –CO–, and –COOH groups, having a residue of 69.1% at 800 °C [346]. In case of RGO-PAniNTs nanocomposites, the onset of second degradation is shifted to higher temperature as compared to that for PAniNTs signifying better thermal stability of the nanocomposites. Consequently, a mass loss of 39% at 800 °C is observed for 40 wt. % nanocomposite as compared to 57% for pure PAniNTs. The decrease in thermal degradation rate of the nanocomposites indicates that the incorporation of RGO within PAniNTs enhances the thermal stability of the nanocomposites. It can be attributed that thermally stable RGO resists the thermal degradation of PAni chains up to a certain temperature range, which leads to an increase in thermal stability of the nanocomposites with increasing RGO concentration.

The derivative thermographs of TG curves are shown in blue in Figure 6.5. From the plot, the onset decomposition (T_{onset}) and rapidest decomposition (T_{rpd}) temperatures for the second degradation have been calculated and summarized in Table 6.3. T_{onset} is the temperature at which degradation starts and T_{rpd} represents the temperature of maximum rate of degradation. RGO does not exhibit the onset and rapidest decomposition temperatures as it does not degrade in the temperature range (50-800 °C) of investigation. It is observed from the table that for pure PAniNTs, T_{onset} = 200 °C and T_{rpd} = 282 °C, while for the nanocomposites T_{onset} and T_{rpd} starts from 376 °C and 561 °C, respectively. This indicates that the rate of decomposition is low in the nanocomposites as compared to pure PAniNTs. It is observed that with increasing concentration of RGO, T_{onset} and T_{rpd} increase attaining highest values for 40 wt. % of RGO concentration. All these results ascertain that the thermal stability of the nanocomposites increases steadily with RGO loading. This is attributed to the fact that the presence of RGO acts as a mass transport barrier to the volatile species of PAniNTs during decomposition giving rise to an increase in thermal stability of the nanocomposites [298].

Table 6.3: *T_{onset}, T_{rpd} and % of residue at 800 °C of RGO, PAniNTs and RGO-PAniNTs nanocomposites*

Sample	T_{onset} (°C)	T_{rpd} (°C)	Residue at 800 °C (%)
RGO	–	–	69.16
PAniNTs	200	282	42.23
5 wt. % RGO	376	561	54.52
10 wt. % RGO	382	579	57.29
20 wt. % RGO	389	583	59.12
40 wt. % RGO	392	586	67.61

6.5 Current-voltage (I-V) characteristics

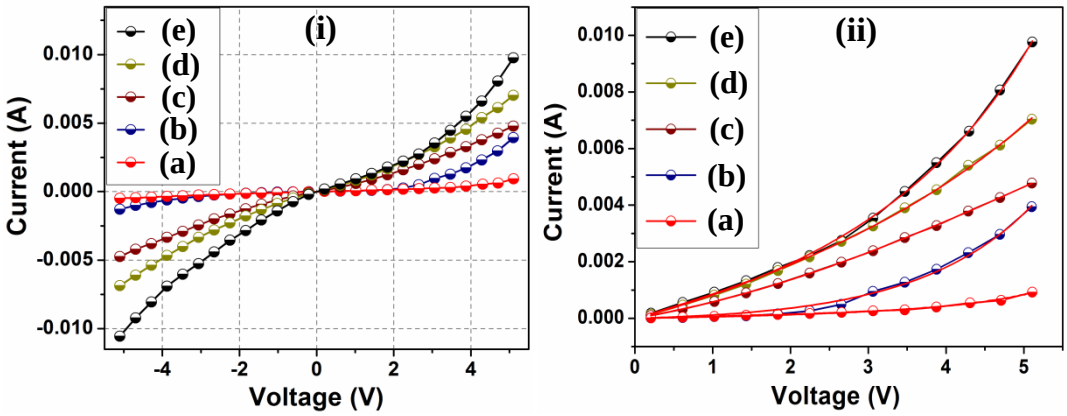

Figure 6.6: *(i) I-V characteristics and (ii) Kaiser equation fitted positive sides of I-V characteristic curves of (a) PAniNTs and RGO-PAniNTs nanocomposites with (b) 5 wt. %, (c) 10 wt. %, (d) 20 wt. % and (e) 40 wt. % of RGO.*

The I-V characteristics of PAniNTs and RGO-PAniNTs nanocomposites are presented in Figure 6.6 (i). These characteristics indicate a significant increase in current with an increase in RGO concentration in the nanocomposites. Conducting polymers, which comprise of both crystalline and amorphous regions, the charge transport occurs by hopping of charge carriers along the polymer chains. The presence of amorphous regions causes charge carrier scattering decreasing their mobility. RGO being highly conducting, the incorporation of RGO in the PAni matrix provides conductive pathways [297]. The RGO nanosheets distributed throughout the PAni matrix helps in forming conductive islands, which increase the hopping sites for charge carriers and facilitates the charge carrier motion. With

increase in the concentration of RGO, the number of conductive islands increases leading to increase in the mobility of charge carriers in the nanocomposites giving rise to enhanced conduction. It is observed from the figure that the I-V characteristics are non-linear and symmetric with respect to the polarity of the applied voltage. The observed non-linear behavior of the I-V characteristics is attributed to the disordered structure of the nanocomposites consisting of crystalline RGO sheets separated by amorphous PAniNTs matrix. The non-linear I-V characteristics are studied by the model proposed by Kaiser et al. given by equation (2.24). Since the I-V characteristics are symmetric with the polarity of the applied voltage, therefore only the positive sides of the I-V curves are considered for fitting. The fitted curves are shown in red solid lines in Figure 6.6 (ii) and the fitting parameters are presented in Table 6.4. It is observed that the low field conductance (G_0) and the parameter h increase as the RGO concentration is increased. This indicates that non-linearity of the I-V curves decreases with increase in RGO concentration and the ohmic component becomes dominant at high RGO loading. The increase in the value of voltage scale factor (V_0) also indicates the minimized non-linearity in the I-V characteristics as the RGO content increases [224].

Table 6.4: *Fitting parameters to Kaiser equation for PAniNTs and RGO-PAniNTs nanocomposites with different RGO concentrations*

Sample	G_0(S)	V_0 (V)	h
PAniNTs	2.23×10^{-4}	1.92	0.70
5 wt. % RGO	2.93×10^{-4}	2.13	0.75
10 wt. % RGO	5.17×10^{-4}	2.93	0.81
20 wt. % RGO	6.73×10^{-4}	3.07	0.87
40 wt. % RGO	9.71×10^{-4}	3.93	0.91

6.6 Conductivity measurements

Electrical conductivities of RGO, PAniNTs and RGO-PAniNTs nanocomposites have been calculated from equation (2.26) at room temperature. The conductivity of pure RGO and PAniNTs is measured to be 9.21 and 0.61 S cm^{-1}, respectively. It is found that RGO-PAniNTs nanocomposites exhibit much higher conductivity than that of PAniNTs. The highest conductivity is calculated to be 8.04 S cm^{-1} for 40 wt.

% of RGO, which is due to the presence of higher concentration of conductive RGO within PAniNTs matrix. The measured conductivity values for the nanocomposites with 5, 10 and 20 wt. % of RGO are 2.18, 4.72 and 7.58 S cm^{-1}, respectively. The large aspect ratio of *in situ* reduced RGO provides a conductive pathway between the low conductive components of PAniNTs, which eases the charge carrier motion giving rise to improved conductivity.

6.7 Electrochemical properties

6.7.1 Cyclic voltammetry

The CV curves of PAniNTs and RGO-PAniNTs nanocomposites in 1 M KCl electrolyte at different voltage scan rates in the potential range of –0.2-0.8 V are shown in Figure 6.7. The CV curve of PAniNTs demonstrates two redox peaks that are attributed to the redox transitions of PAni, which signifies its pseudocapacitive behavior. The oxidation peaks are observed at 0.23 V and 0.52 V that corresponds to the leucoemeraldine-emeraldine and emeraldine-pernigraniline transformations of PAni, respectively [347]. Similarly, there are two corresponding reduction peaks at 0.45 V and 0.09 V in the reverse potential scan. For RGO-PAniNTs nanocomposites also, the two redox peaks are observed indicating the contribution of pseudocapacitance. Upon incorporation of RGO, the CV loops of the nanocomposites display a larger enclosed area and high current response, suggesting the increase of specific capacitance and their potential as supercapacitor electrodes. With increase in the concentration of RGO, the intensity of PAni redox peaks decreases, which is attributed to the increasing EDL charge storage contribution from RGO. The nanocomposite with 40 wt. % of RGO exhibits the highest current response with nearly rectangular CV shape and distinct PAni redox peaks as shown in Figure 6.7 (e). It is noticed that the anodic peaks shift positively and the cathodic peaks shift negatively with increasing potential scan rate from 10 to 100 mV s^{-1}. The shape of the nearly rectangular CV is maintained even at higher scan rates. The increase in charge storage capacity results from the synergistic effect of the interactions of RGO and PAniNTs that collectively give rise to EDLC and faradaic capacitance in the nanocomposites. RGO provides a highly conductive network for PAniNTs that eases the charge carrier motion in the nanocomposite electrodes. In addition, the nanotube-shaped PAni on the RGO nanosheets helps in preventing the

aggregation of RGO, allowing more exposed surface area to be accessible to the electrolyte.

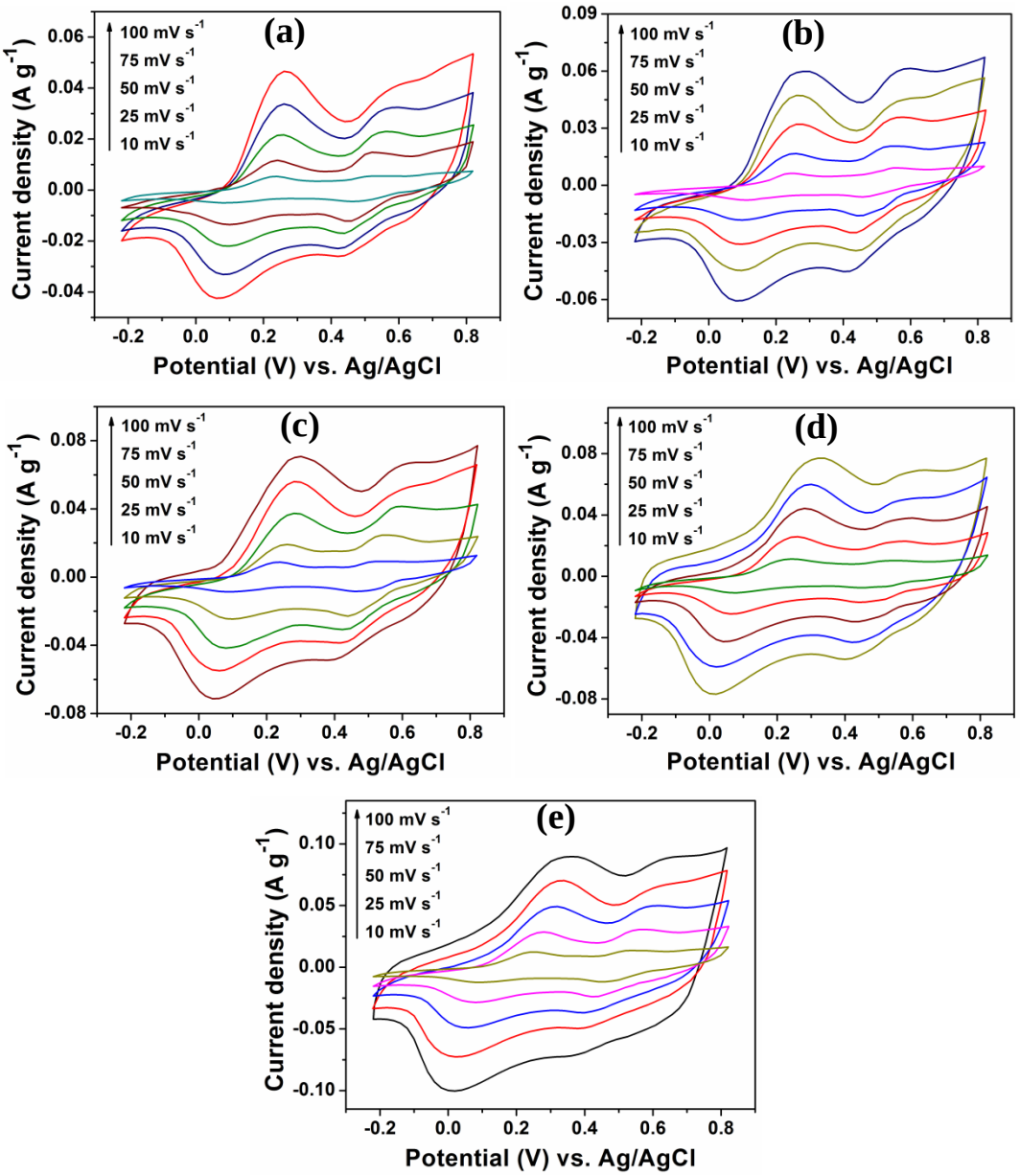

Figure 6.7: *CV curves at different voltage scan rate of (a) PAniNTs and RGO-PAniNTs nanocomposites with (b) 5 wt. %, (c) 10 wt. %, (d) 20 wt. % and (e) 40 wt. % of RGO.*

6.7.2 Galvanostatic charge-discharge measurements

The GCD measurements of RGO, PAniNTs and RGO-PAniNTs nanocomposites have been performed in the voltage range of 0–0.8 V in 1 M KCl electrolyte at a constant current density of 0.5 A g^{-1} and are displayed in Figure 6.8 (i).

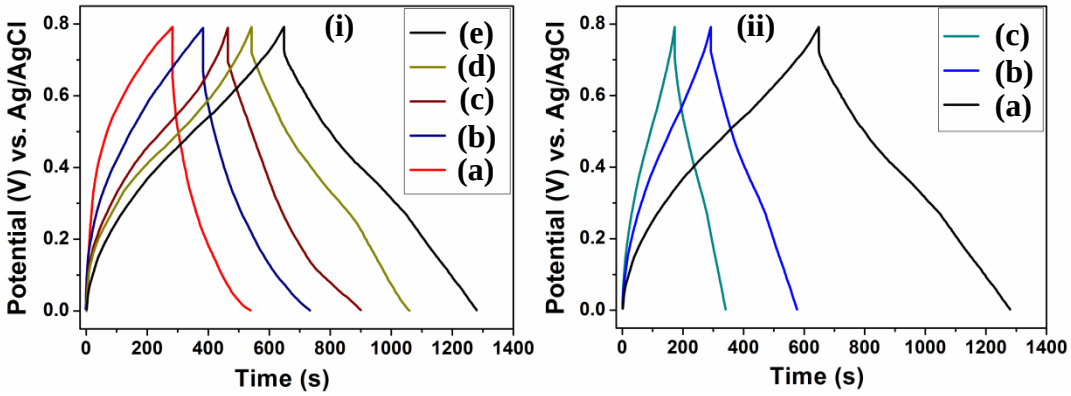

Figure 6.8: *(i) GCD curves of (a) PAniNTs and RGO-PAniNTs nanocomposites with (b) 5 wt. %, (c) 10 wt. %, (d) 20 wt. % and (e) 40 wt. % of RGO at a current density of 0.5 A g^{-1}; (ii) GCD curves of 40 wt. % RGO-PAniNTs nanocomposite at a current density of (a) 0.5 A g^{-1}, (b) 1 A g^{-1} and (c) 1.5 A g^{-1}.*

The discharge curve of PAniNTs shows a shorter and fast discharge and deviates from linearity which indicates the faradaic pseudocapacitive feature of the electrode [348]. For the nanocomposites up to a concentration of 10 wt. % of RGO, the discharge curves are non-linear similar to that for pure PAniNTs, which may be due to the dominant pseudocapacitive mechanism in the electrode resulting from PAniNTs as the amount of RGO is much lower (10 wt. %) than that of PAniNTs. However, the GCD curve of the nanocomposites with higher loading of RGO (20 and 40 wt. %) shows two different discharge behavior. Initially, linear and faster discharge is observed in the potential range of 0.8-0.4 V followed by a slower discharge that deviates from the initial linear behavior. The initial linear discharge curve is exhibited by EDLC materials and may be attributed to the EDLC characteristics of the electrode due to RGO in the nanocomposites [233]. The latter slower discharge, not observed for pure PAniNTs, may arise from the combination of EDLC (due to RGO) and pseudocapacitance (due to PAniNTs) in the nanocomposites. The specific capacitance (C_{sp}) and coulombic efficiency (η) have been evaluated from the GCD curves using the equations given below:

$$C_{sp} = \frac{I\Delta t_d}{m\Delta V} \tag{6.2}$$

$$\eta = \frac{\Delta t_d}{\Delta t_c} \times 100\% \tag{6.3}$$

where m is the mass of the electrode material, I is the applied constant current, ΔV is the discharge potential and Δt_d and Δt_c are the discharging and the charging times, respectively. The obtained values of C_{sp} and η are listed in Table 6.5. A maximum specific capacitance of 448.57 F g^{-1} is obtained for 40 wt. % RGO-PAniNTs nanocomposites, which is much higher than 194.65 F g^{-1} of that of PAniNTs.

Table 6.5: *Specific capacitance, energy density, power density, coulombic efficiency, equivalent series resistance (R_s) and charge transfer resistance (R_{ct}) of PAniNTs and RGO-PAniNTs nanocomposites*

Sample	**Specific capacitance (F g^{-1})**	**Energy density (W h kg^{-1})**	**Power density (W kg^{-1})**	**Coulombic efficiency**	**R_s (Ω)**	**R_{ct} (Ω)**
PAniNTs	194.65	11.59	163.62	90%	11.13	32.19
5 wt. % RGO	264.19	15.98	164.83	91%	11.06	23.33
10 wt. % RGO	321.48	20.34	168.71	93%	9.53	13.51
20 wt. % RGO	372.46	24.62	172.43	95%	7.82	7.74
40 wt. % RGO	448.57	30.52	174.96	97%	5.29	4.05

The GCD curves for 40 wt. % of RGO-PAniNTs electrode at different current densities are shown in Figure 6.8 (ii). The longer discharge duration of the nanocomposites implies improved specific capacitance and energy storage. The internal resistance (IR drop) is reduced in the electrode, which is of crucial importance for electrodes producing less heat during charging and discharging [349]. High coulombic efficiency is also desired in electrodes that determines the electrochemical reversibility of the electrode materials. In this case, the highest coulombic efficiency is measured to be 97% for the nanocomposite with 40 wt. % of RGO as compared to 90% for PAniNTs. The presence of RGO in the nanocomposites enhances the total specific capacitance by providing a capacitive double layer for charge storage and simultaneously a high surface area backbone that increases the contact between the electrode and electrolyte. The agglomeration of RGO nanosheets is minimized by the presence of PAniNTs onto the RGO sheets that act as spacers, which improves the permeation of the electrolyte into the electrode. Moreover, the tubular morphology of polyaniline over the RGO surface plays a

major role in increasing the specific capacitance of the hybrid composite by providing both inner and outer contact area with the electrolyte and shortening the electrolyte ion transport pathlengths throughout the electrode. Thus the complementary properties of both the components produce a synergistic effect to enhance the electrochemical performance. The energy density and power density values are calculated from the GCD curves according to the equations (2.30) and (2.31), respectively and are tabulated in Table 6.5. A high energy density of 30.52 W h kg^{-1} at a power density of 174.96 W kg^{-1} is achieved for the nanocomposite with 40 wt. % of RGO at a current density of 0.5 A g^{-1}.

6.7.3 Electrochemical impedance spectroscopy

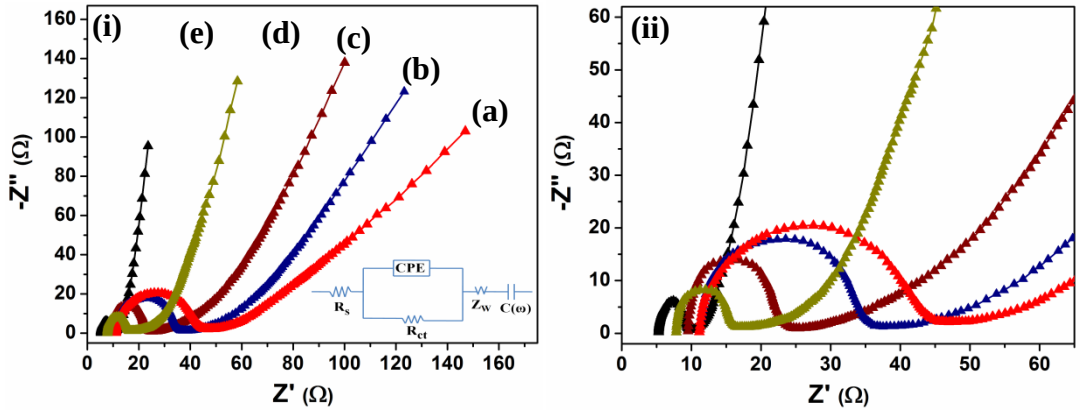

Figure 6.9: *(i) Nyquist plots of (a) PAniNTs and RGO-PAniNTs nanocomposites with (b) 5 wt. %, (c) 10 wt. %, (d) 20 wt. % and (e) 40 wt. % of RGO (Inset shows equivalent circuit) and (ii) Magnified view of the Nyquist plot in Z' range of 0 to 65 Ω.*

The EIS have been conducted to measure the different types of internal resistances of the electrodes in the frequency range of 10 mHz to 50 kHz at room temperature. The Nyquist plots are shown in Figure 6.9 (i) where a small arc in the high frequency region followed by a vertical line at low frequency is observed. The Nyquist plots have been analyzed based on Randles equivalent circuit as shown in the inset, which comprise of equivalent series resistance (R_s), charge transfer resistance (R_{ct}) and interface resistance (CPE) in the high frequency region and Warburg impedance (Z_w) and supercapacitor cell capacitance ($C(\omega)$) in the low frequency region, respectively. The R_s is estimated from the x-intercept of the arc and is presented in Table 6.5. The

R_s of the nanocomposites are found to decrease as the concentration of RGO is increased. This indicates low electrode and electrolyte resistance in case of the nanocomposites which could be ascribed to the presence of highly conductive RGO. The presence of the semicircle at the high frequency range signifies that there is some discontinuity in the charge transfer process [350]. However, the diameter of the semicircle decreases in the nanocomposites as seen from the magnified plots [Figure 6.9 (ii)], which indicates low R_{ct} in the nanocomposites. The slope of the 45° line in the lower frequency region is Z_w that represents the resistance during the diffusion process of the electrolyte ions [348]. The decreased 45° slope for the nanocomposites indicates lower variations in ion diffusion pathlengths in the nanocomposite electrode as compared to PAniNTs. The nearly vertical line parallel to the y-axis at low frequency observed for 40 wt. % RGO-PAniNTs nanocomposite electrode demonstrates purely capacitive behavior.

6.7.4 Cyclic stability study

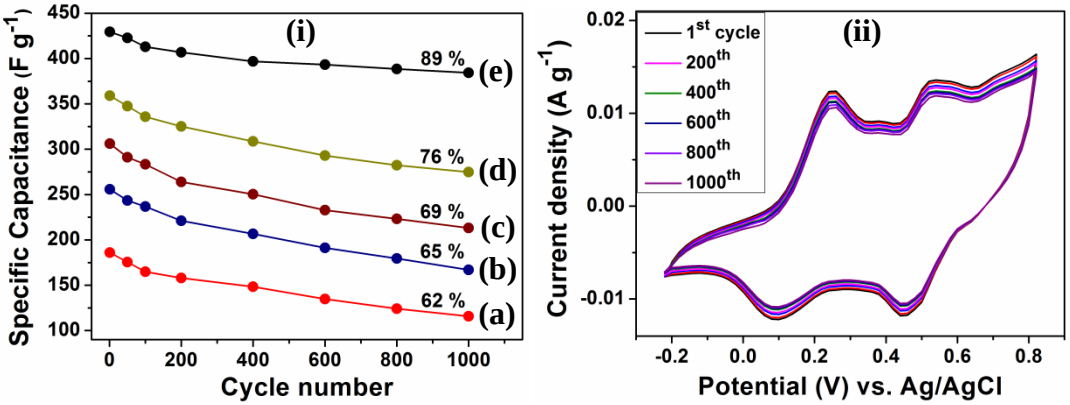

Figure 6.10: *(i) Variation of specific capacitance with cycle number of (a) PAniNTs and RGO-PAniNTs nanocomposites with (b) 5 wt. %, (c) 10 wt. %, (d) 20 wt. % and (e) 40 wt. % of RGO; (ii) CV curves with increasing cycle number of 40 wt. % RGO-PAniNTs nanocomposite.*

The electrochemical stability of PAniNTs and RGO-PAniNTs nanocomposites has been tested by repeating the CV measurements at a scan rate of 10 mV s^{-1} for 1000 cycles. The specific capacitance values of PAniNTs and the nanocomposites have been calculated with increasing number of CV cycles using equation (2.38) and are shown in Figure 6.10 (i). PAniNTs electrode exhibits a capacitive retention of 62%

after 1000 cycles. The cyclic stability increases upon incorporation of RGO and the nanocomposite electrode with 40 wt. % of RGO exhibits the highest cyclic stability of 89% after 1000 cycles. The 20 wt. % RGO-PAniNTs nanocomposite electrode also delivers an improved capacitive retention of 76% after 1000 cycles. The CV curves of 40 wt. % RGO-PAniNTs nanocomposite electrode with increasing cycle number are displayed in Figure 6.10 (ii). It is observed that the shape and area of the enclosed curve are retained even after 1000 cycles suggesting good cyclic stability.

6.8 Summary

Nanocomposites of RGO and PAniNTs have been synthesized by *in situ* reduction of GO in presence of PAniNTs that act as spacers between RGO sheets. HRTEM micrographs depict sheet-like morphology of RGO and an average diameter of PAniNTs around 134 nm. X-ray diffraction patterns show a broad peak at $2\theta = 15°$-$28°$ in the nanocomposites due to overlapping of the (002) peak of RGO with the (020) and (200) peaks of PAniNTs. The appearance of (100) peak of RGO at $2\theta = 43°$ in the XRD patterns of 20 wt. % and 40 wt. % RGO-PAniNTs nanocomposites signify the *in situ* reduction of RGO in presence of PAniNTs. An increase in crystallinity is obtained with increase in RGO concentration from 26% for pure PAniNTs to 44% for the RGO-PAniNTs nanocomposite with 40 wt. % of RGO. FTIR spectra of the nanocomposites display shifting of bands of PAniNTs at 1562, 1477, 1107 and 795 cm^{-1} towards higher wave numbers of 1587, 1496, 1130 and 814 cm^{-1}, respectively in the nanocomposites indicating π-π interaction between PAni chains and RGO nanosheets. Micro-Raman spectra depict all the characteristic peaks of RGO and PAniNTs in the nanocomposites. A red shifting in the C-H bending and C-N stretching vibrations of PAni occurs from 1196 to 1180 cm^{-1} and 1266 to 1233 cm^{-1}, respectively in the Raman spectra of the nanocomposites indicating a change in chemical environment of the C-H and C-N bands in the nanocomposite during the *in situ* formation of RGO. This shifting could be attributed to electron cloud delocalization of C-H and C-N bands in the nanocomposite structure due to the presence of RGO. Thermogravimetric studies reveal an enhancement in thermal stability of the nanocomposites with an increase in RGO concentration. The derivative TG curves display higher onset and rapidest decomposition temperatures for the nanocomposites than that for PAniNTs signifying low decomposition rate of

the nanocomposites. This is ascribed to the presence of thermally stable RGO in the nanocomposites that resists the thermal degradation of PAni chains up to a certain temperature range, which leads to the increase in thermal stability of the nanocomposites with increasing RGO concentration. The Kaiser fitting of the I-V characteristics indicates an increase in the values of low field conductance (G_0), voltage scale factor (V_0) and *h* with increase in RGO content. This implies decrease in non-linearity of the I-V curves and the dominant role of ohmic conduction with increase in RGO concentration. Improved conductivity values of the nanocomposites are obtained as compared to PAniNTs, which is due to the large aspect ratio of *in situ* reduced RGO providing a conductive pathway between the low conductive components of PAniNTs for charge carrier motion. The CV curve of PAniNTs exhibits two oxidation peaks at 0.23 V and 0.52 V that correspond to the leucoemeraldine-emeraldine and emeraldine-pernigraniline faradaic reactions of PAni, respectively signifying its pseudocapacitive characteristics. Similarly, there are two corresponding reduction peaks at 0.45 V and 0.09 V in the reverse cycle. The nanocomposites display an enhanced CV area and current response upon incorporation of RGO, which indicates improved charge storage characteristics. The intensity of the PAni redox peaks decreases, while the current response and enclosed CV area increases with increase in RGO concentration, which demonstrates increasing EDL charge storage contribution from RGO in the nanocomposites. GCD curves reveal the dominant contribution of pseudocapacitance in the nanocomposites upto a RGO concentration of 10 wt. %. With increase in RGO loading to 20 and 40 wt. %, the combination of both EDLC and pseudocapacitance is observed in the discharge curves of the nanocomposites. The highest specific capacitance of 448 Fg^{-1} with a coulombic efficiency of 97% is achieved from the GCD curves for the nanocomposite with 40 wt. % of RGO. The highest energy density and power density values of 30 W h kg^{-1} and 174 W kg^{-1}, respectively are obtained for 40 wt. % RGO-PAniNTs nanocomposite. EIS studies reveal lower R_s and R_{ct} values for the nanocomposites than that for PAniNTs, which indicates low interfacial contact and charge transfer resistances of the nanocomposites. The lowest R_s and R_{ct} values of 5.29 Ω and 4.05 Ω, respectively are recorded for the nanocomposite with a RGO concentration of 40 wt. %. PAniNTs deliver an electrochemical stability of 62% after 1000 cycles, which increases as the RGO concentration is increased. A high capacitive retention of 89% after 1000 cycles is achieved for 40 wt. % RGO-

PAniNTs nanocomposite, which arises due to the synergistic effect of EDLC (from RGO) and pseudocapacitance (from PAniNTs) in the nanocomposite.